COMMUNICATION

Efficient Flexible Organic/Inorganic Hybrid Perovskite Light-Emitting Diodes Based on Graphene Anode

*Hong-Kyu Seo, Hobeom Kim, Jaeho Lee, Min-Ho Park, Su-Hun Jeong, Young-Hoon Kim, Sung-Joo Kwon, Tae-Hee Han, Seunghyup Yoo, and Tae-Woo Lee**

Organic/inorganic hybrid perovskites (OIPs) are promising light-emitting materials for perovskite light-emitting diodes (PeLEDs) due to high color purity, low material cost, tunable band gap, and easy fabrication.[1–4] However, OIPs have intrinsic problems of long exciton diffusion length L_D (>100 nm for pure OIPs, and >1 μm for mixed OIPs) and small exciton binding energy (<100 meV) which have been known as the fundamental reason for very weak electroluminescence (EL) at room temperature.[2,5,6] Recently, the EL intensity of PeLEDs has been improved drastically based on 3D methylammonium lead halide ($MAPbX_3$, where X is I, Br, or Cl) and $MAPb(Br_{1-x}Cl_x)_3$ emitting layer (EML), or quasi-2D perovskite EML by mixing phenylethyl ammonium lead bromide ($(PEA)_2PbBr_4$) with $MAPbBr_3$: some PeLEDs that use an $MAPbBr_3$ green EML have achieved bright electroluminescence with maximum luminance L_{max} > 100 cd m^{-2} or even >1000 cd m^{-2} at room temperature.[2,3,7–11] These PeLEDs were based on an indium tin oxide (ITO) anode which is the conventional transparent conductive oxide (TCO) electrode in optoelectronic devices. However, the price of In is increasing due to the limited availability of In sources.[12] In addition, ITO is brittle, so it is not readily applicable in highly flexible PeLEDs.[2,12] Furthermore, release of metallic In and Sn species from the ITO into overlying layers can cause quenching of excitons which is more serious in PeLEDs having long L_D.[13–16] Therefore, finding a flexible and chemically inert ITO-free electrode that can realize highly efficient flexible PeLEDs is very important. However, few studies on TCO-free flexible PeLEDs have been conducted. The printed PeLEDs on CNT/polymer substrate with printed Ag nanowire electrode have the advantages of being flexible and roll-to-roll processable, but they showed relatively low device efficiency (maximum current efficiency CE_{max} = 0.6 cd A^{-1}, and maximum external quantum efficiency EQE_{max} = 1.1%) with L_{max} of ≈200 cd m^{-2}.[17]

Among the various flexible electrodes,[18–23] graphene is a promising candidate as a flexible anode due to its high transparency, high conductivity, low cost, and chemical stability.[24–31] Therefore, perovskite solar cells (PSCs) with graphene electrodes have recently been demonstrated,[23,32–35] and TCO-free PSCs based on a graphene anode achieved comparable efficiency to that of an ITO-based device.[23] However, because the devices were fabricated on a glass substrate, they could not take advantage of the flexible graphene electrodes. Therefore, the fabrication of PeLEDs with a graphene anode (Gr-PeLEDs) that achieve higher device efficiency and better flexibility than that of ITO-based PeLEDs (ITO-PeLEDs) would be a significant advance in flexible perovskite optoelectronic devices.

Here, we achieved highly efficient ITO-free and flexible organic/inorganic hybrid PeLEDs with very bright EL (L_{max} > 10 000 cd m^{-2}) and high efficiency (CE_{max} = 18.0 cd A^{-1}) based on a graphene anode for the first time. Four-layer graphene (4LG) films with a self-organized gradient buffer hole-injection layer (Buf-HIL; formerly, we also called GraHIL in organic light-emitting diodes (OLEDs)) (a composition composed of poly(3, 4-ethylenedioxythiophene):poly(styrene sulfonate) (PEDOT:PSS) and a perfluorinated ionomer (PFI))[13,14] and an $MAPbBr_3$ emitter were used to make green-emitting PeLEDs. To overcome the low device efficiency of PeLEDs, we used additive-based nanocrystal pinning, which can modify the $MAPbBr_3$ EML and thus results in high-efficiency PeLEDs.[1] We still suffered from relatively low device efficiency of ITO-PeLEDs (CE_{max} = 10.6 cd A^{-1} and EQE_{max} = 2.2%), even though we previously achieved a high efficiency in the ITO-free PeLED using a self-organized conducting polymer (SOCP) anode.[1] However, the Gr-PeLEDs showed much higher CE_{max} = 18.0 cd A^{-1} and EQE_{max} = 3.8% than did ITO-PeLEDs, which implies that the device using a graphene electrode excludes the adverse effect of ITO electrode in terms of exciton quenching caused by the In and Sn species migrated into the Buf-HIL.[13–16]

To fabricate the graphene anode for PeLEDs, graphene was grown using chemical vapor deposition on Cu foil, then transferred to a glass substrate by a conventional graphene transfer process; 4LG was prepared by repeating the transfer process.[36] 4LG that had been chemically p-type doped using HNO_3 vapor had sheet resistance R_S = 84.2 ± 2.7 Ω sq^{-1} (pristine 4LG: R_S = 225.7 ± 6.0 Ω sq^{-1}).[14] Raman spectrum of D-to-G band peak intensity ratio (I_D/I_G < 0.1) and Raman mapping confirmed that both pristine and HNO_3 doped 4LG were of high quality and had few defects (Figure S1a,b, Supporting Information).[25,26]

H.-K. Seo, H. Kim, M.-H. Park, S.-H. Jeong, S.-J. Kwon
Department of Materials Science and Engineering
Pohang University of Science and Technology (POSTECH)
77 Cheongam-Ro, Nam-Gu, Pohang
Gyeongbuk 790-784, Republic of Korea
J. Lee, Prof. S. Yoo
School of Electrical Engineering
Korea Advanced Institute of Science and Technology (KAIST)
Daejeon 305-701, Republic of Korea
Dr. Y.-H. Kim, Dr. T.-H. Han, Prof. T.-W. Lee
Department of Materials Science and Engineering
Seoul National University
1 Gwanak-ro, Gwanak-gu, Seoul 08826, Republic of Korea
E-mail: twlees@snu.ac.kr, taewlees@gmail.com

DOI: 10.1002/adma.201605587

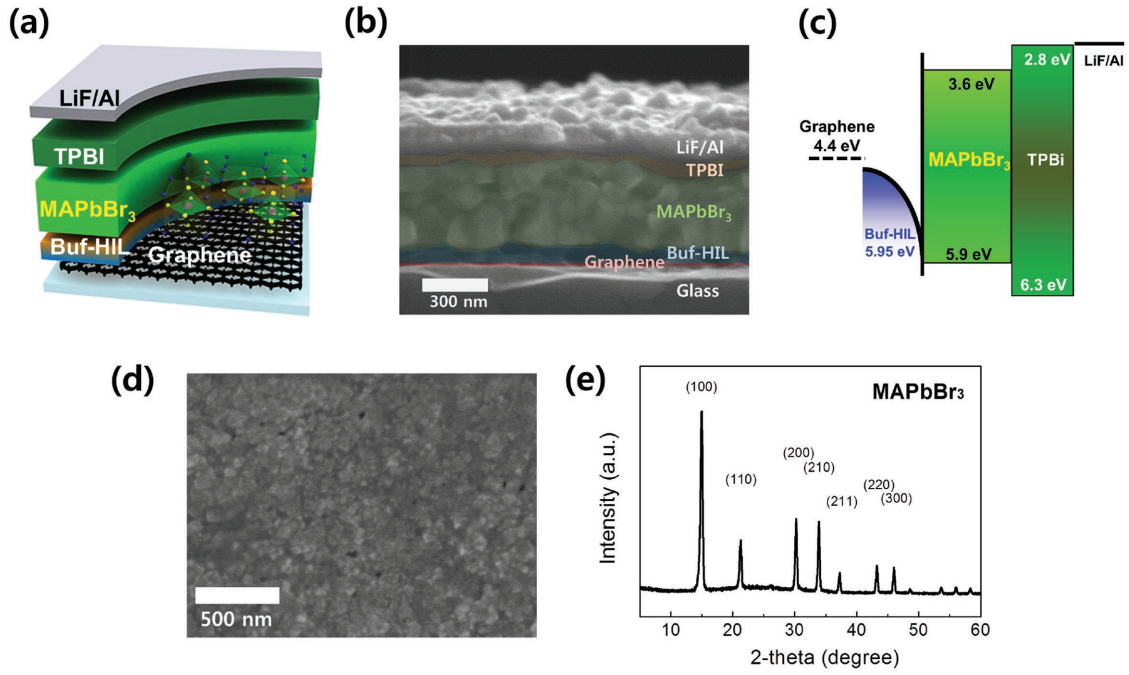

Figure 1. a) Device structure of PeLED with graphene electrode (Gr-PeLED) and $MAPbBr_3$ emitter. b) Cross-sectional scanning electron microscope (SEM) image and c) energy band structure of Gr-PeLED. d) SEM image and e) X-ray diffraction (XRD) pattern of $MAPbBr_3$ film.

We fabricated Gr-PeLEDs with a $MAPbBr_3$ emitter; their structure was 4LG/Buf-HIL (100 nm)/$MAPbBr_3$ (400 nm)/2,2′,2″-(1,3,5-benzinetriyl)-tris(1-phenyl-1-H-benzimidazole) (TPBi) (50 nm)/LiF (1 nm)/Al (110 nm) (**Figure 1**a). The components of the device were carefully deposited, and its layered structure can be confirmed in the cross-sectional image obtained with scanning electron microscopy (SEM) (Figure 1b). We also fabricated ITO-PeLEDs with the same structure. The Buf-HIL layer was spin-coated on 4LG. The work function (WF) of the Buf-HIL gradually increases from the bottom surface (≈5.2 eV) to the top surface (≈5.95 eV) due to the gradually enriched self-organized PFI. Therefore, Buf-HIL can mediate Ohmic contact between anode and EML even though graphene has relatively lower WF (≈4.4 eV) than that of ITO (≈4.7 ≤ WF ≤ ≈4.9 eV) (Figure 1c).[13,14] The $MAPbBr_3$ layer was formed on the Buf-HIL by spin-coating an $MAPbBr_3$ precursor solution. To crystallize the perovskite, the nanocrystal pinning method was applied.[1,37] The $MAPbBr_3$ film had very small grain size (Figure 1d), as in a previous report.[1] $MAPbBr_3$ film on 4LG/Buf-HIL on ITO/Buf-HIL had sharp X-ray diffraction (XRD) peaks at almost same positions (Figure 1e, and Figure S2 and Table S1, Supporting Information). From the XRD data, the crystallite sizes calculated using the Scherrer equation were 26.7 ± 3.8 nm for of $MAPbBr_3$ on 4LG/Buf-HIL and 27.6 ± 3.1 nm for ITO/Buf-HIL.[1]

To investigate the luminescent property, first we measured steady-state photoluminescence (PL) of $MAPbBr_3$ films on 4LG/Buf-HIL and ITO/Buf-HIL (excitation wavelength: 405 nm) (**Figure 2**a). The PL peak intensity from the $MAPbBr_3$ film was approximately five times higher on 4LG/Buf-HIL than on ITO/Buf-HIL, despite $MAPbBr_3$ films being fabricated in the same way; this result implies that the huge difference in PL intensity is a result of the anode materials.

It is well known that ITO can contaminate the HIL as In and Sn atoms can be released and diffuse from ITO to the upper layers during the formation of an acidic conjugated polymer layer on an ITO anode (e.g., PEDOT:PSS).[13–16] These diffused atoms from ITO can form interfacial trap states that reduce the hole-injection efficiency of the the HIL, and act as luminescence quenching sites that cause metal-induced nonradiative recombination of excitons in EML.[13,14,38,39] However, the graphene anode is very stable chemically and includes no metal, and so these phenomena are less likely to occur. This statement is supported by time-of-flight secondary ion mass spectrometry (TOF-SIMS) depth profiles measured from the top of $MAPbBr_3$ films to the bottom of the Buf-HIL (**Figure 3**a,b).[40] Films on ITO and graphene both showed the signals of Pb^+ and CF^+ ion that represent the $MAPbBr_3$ and Buf-HIL layer, respectively, and the interface of Buf-HIL and $MAPbBr_3$ is revealed after sputtering time ≈300 s. The sample on ITO anode shows clear In and Sn signals that gradually decreased from the top of ITO to the interface between the Buf-HIL and $MAPbBr_3$ layer (Figure 3a), but the sample on the 4LG anode showed no signal of In or Sn as well as other contaminants (Figure 3b). The depth profile of In atoms from the top surface to the bottom of Buf-HIL layer on the ITO anode demonstrated that a lot of In species already have migrated into the Buf-HIL and to the top surface of Buf-HIL before the formation of $MAPbBr_3$ layer on Buf-HIL (Figure S3, Supporting Information).[14]

To verify the effects of the different anodes, we measured time-resolved photoluminescence (TR-PL) of $MAPbBr_3$ films on Buf-HIL with 4LG or ITO, and on a glass substrate without anode, as a reference (Figure 2b). The PL decay curves agree well with a biexponential decay fitting that represents two relaxation mechanisms: fast decay with lifetime τ_1 related to

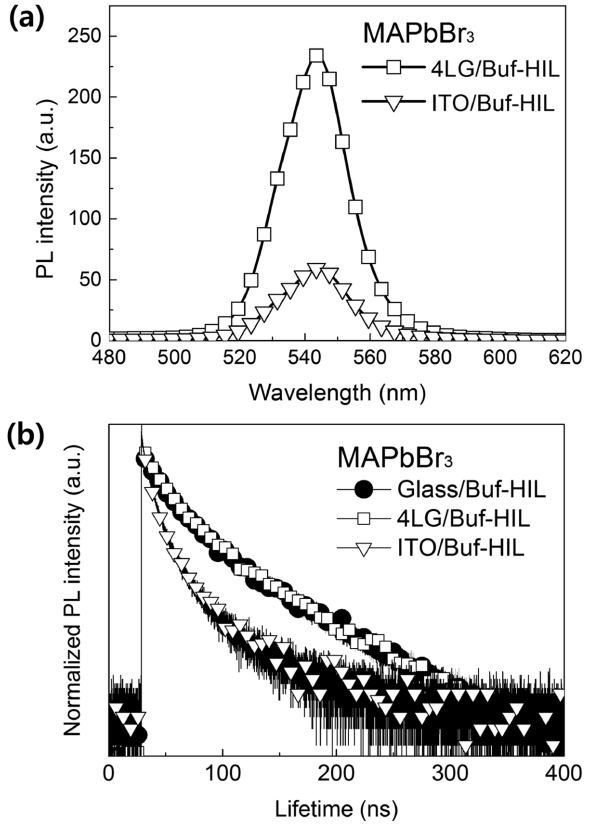

Figure 2. a) Steady-state photoluminescence (PL) spectra of $MAPbBr_3$ film on 4LG/Buf-HIL and ITO/Buf-HIL. b) PL lifetime curves of $MAPbBr_3$ film obtained from time-resolved PL measurement on glass/ graphene/ ITO/Buf-HIL.

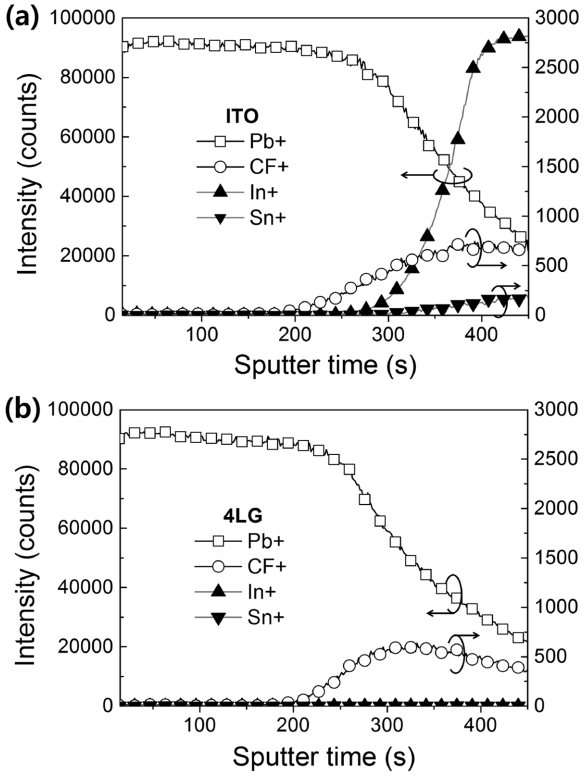

Figure 3. TOF-SIMS depth profiles (from the top of $MAPbBr_3$ films) of Buf-HIL/$MAPbBr_3$ films that have a) ITO and b) 4LG anodes.

nonradiative recombination such as quenching of free carriers or exciton; and slow decay related with lifetime τ_2 that represents radiative recombination.[1] The PL decay curves of glass and 4LG sample decreased slowly and had relatively long average PL lifetime τ_{ave} (4LG: 76.3 ns, glass: 77.6 ns), whereas the PL decay curve of ITO sample decreased quickly, with τ_{ave} = 22.6 ns because the fraction (64.4%) of τ_1 (9.7 ns) was larger than that of τ_2 (45.9 ns) (Table S2, Supporting Information). These results mean that the 4LG and glass samples had much smaller luminescence quenching than ITO sample, because of the absence of diffused In and Sn atoms in 4LG and glass samples resulted in higher PL intensity and longer τ_{ave} than in the ITO sample.

The graphene anode increased the device efficiency. The Gr-PeLEDs showed CE_{max} = 18.0 cd A^{-1}, whereas the ITO-PeLEDs had CE_{max} = 10.6 cd A^{-1} (**Figure 4**a). Furthermore, the Gr-PeLEDs require less current density *J* than the ITO-PeLEDs for the same luminance (Figure 4b). The CE and *L* of Gr-PeLEDs tended to increase as the number of graphene layer increased from mono- to four-layer, which is consistent with the previous literature in OLEDs based on graphene anode (Figure S4, Supporting Information).[14] We also calculated EQE_{max} of PeLEDs by analyzing the angular emission profiles (Figure S5, Supporting Information).[41] The calculated EQE_{max} of Gr-PeLEDs was 3.8%, which is higher than that of ITO-PeLEDs (2.2%). These improved results in Gr-PeLEDs are consistent with the PL study that showed increased PL intensity and extended PL lifetime. The change of the anode from ITO to graphene prevents severe exciton quenching caused by metal atom species that diffuse from ITO into the Buf-HIL.[13,14,38,39] Because the L_D (≈67 nm) of the $MAPbBr_3$ emitter with small grain size (≈100 nm)[1] is still longer than L_D of organic emitters (≈10 nm), these diffused metal atom species inside the Buf-HIL and at its interface with $MAPbBr_3$ layer in the PeLEDs with the simplified device structure similar to polymer LEDs rapidly quench excitons from $MAPbBr_3$.[2,13,14] In OLEDs, the efficiency difference between ITO-OLEDs and Gr-OLEDs is not significant because the L_D of organic emitters is very short and the exciton binding energy is large (>200 meV).[2,6,13,14] However, the efficiency difference between ITO-PeLEDs and Gr-PeLEDs is much larger because of very long L_D and small exciton binding energy of the perovskite emitters. Therefore, to achieve highly efficient PeLEDs, the chemically inert electrode is essential for the $MAPbBr_3$ emitter having long L_D. Schematic drawings (Figure 4c) effectively show the mechanism of exciton quenching by In and Sn atoms in detail. The EL spectrum of PeLEDs showed green emission centered at 542 nm; the narrow peaks (full width half maximum = 21 nm) verify the high color purity of PeLEDs with the $MAPbBr_3$ emitter (Figure 4d,e). However, one thing we need to discuss is that the efficiency of Gr-PeLED is still lower than that of SOCP-PeLED (CE_{max} = 42.9 cd A^{-1}, EQE_{max} = 8.5%), even though both SOCP and graphene did not release metallic species.[1] This difference may be ascribed to different surface properties between the SOCP film and the Buf-HIL leading to different

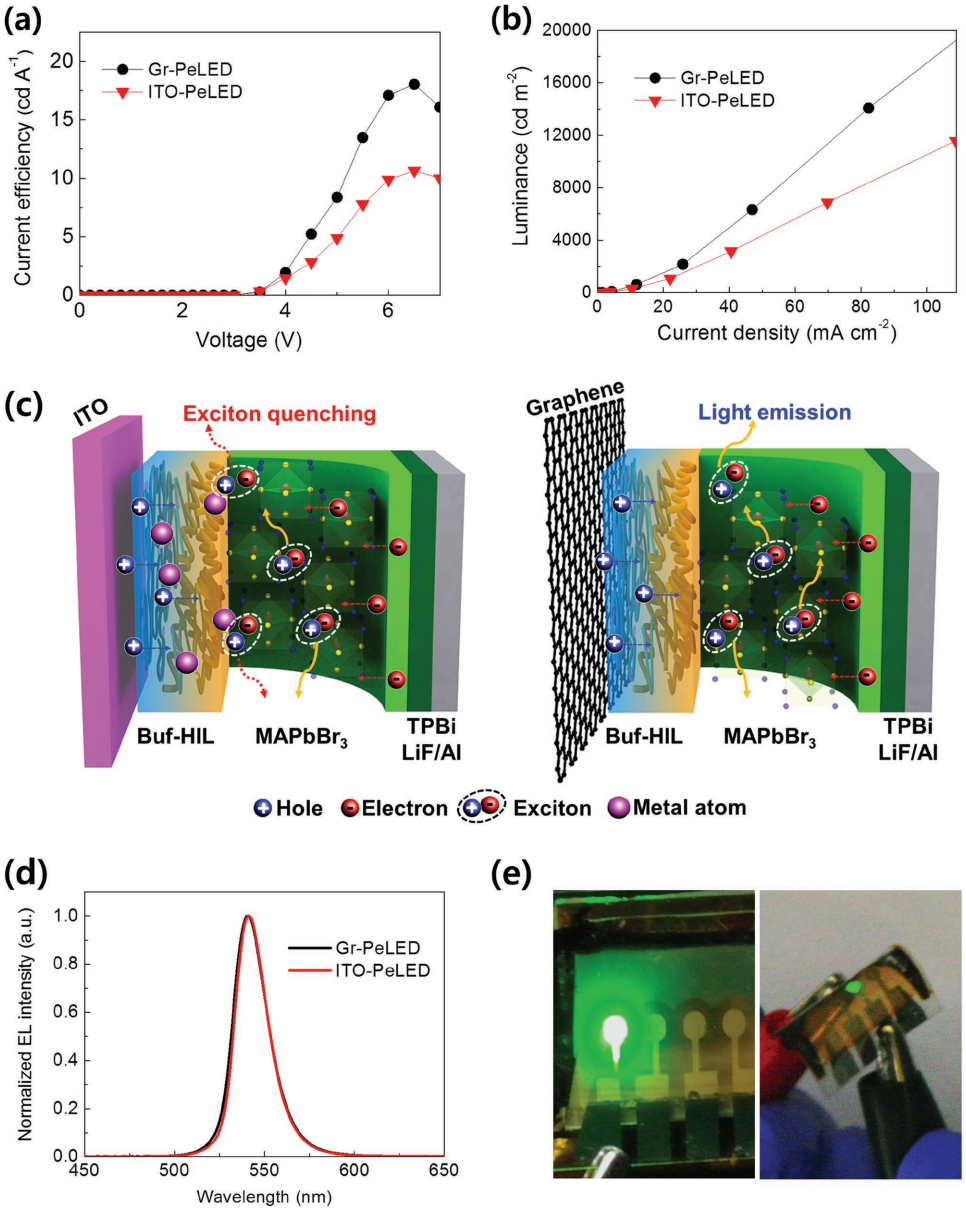

Figure 4. a) Current efficiency and b) luminance of Gr-PeLED and ITO-PeLED. c) Schematic drawings of exciton quenching by In and Sn atoms in ITO-PeLEDs (left), and efficient light emission in Gr-PeLEDs (right). d) Electroluminescence (EL) spectra of Gr-PeLED and ITO-PeLED. e) Photograph of flexible green-emitting Gr-PeLEDs on glass (left) and PET substrate (right).

growth of perovskite polycrystals, and different optical out-coupling effect related to light extraction due to the different device structures which we need to investigate further.

To exploit the high flexibility of graphene and its superior property as an anode, we also fabricated flexible Gr-PeLEDs on a plastic substrate (Figure 4e). These Gr-PeLEDs showed high $CE_{max} = 16.1$ cd A^{-1} and $L_{max} \approx 13\,000$ cd m^{-2} with high bending stability (Figure S6, Supporting Information). To demonstrate the mechanical robustness of flexible graphene anode, we tested the bending stability of flexible Gr- and ITO-PeLEDs on polyethylene terephthalate (PET) substrate[2,14] under repeated bending events with 1.34% strain (bending radius of 7.5 mm for a 200 μm thick substrate).[42] The J of flexible Gr-PeLEDs decreased slightly to ≈81% of initial J after 1200 bending cycles (**Figure 5**a). However, due to the brittleness of ITO anode, J of flexible ITO-PeLEDs decreased significantly (to ≈64%) after only 200 cycles, and failed completely by the 1200 bending cycles.[14] We also performed a flexibility test with gradually reduced bending radius of flexible PeLEDs from 0.7 to 5.3% strain that have 4LG and ITO anode. The Gr-PeLEDs endured a bending strain of 5.3% (bending radius of 1.9 mm) without significant change of J, whereas in ITO-PeLEDs the gradual increase of bending strain caused severe decrease of J, and a bending strain of 5.3% resulted in complete failure (Figure 5b).[43] Therefore, flexible Gr-PeLEDs have reliable bending stability and flexibility to fabricate rollable displays that require a 5–10 mm bending radius.[44]

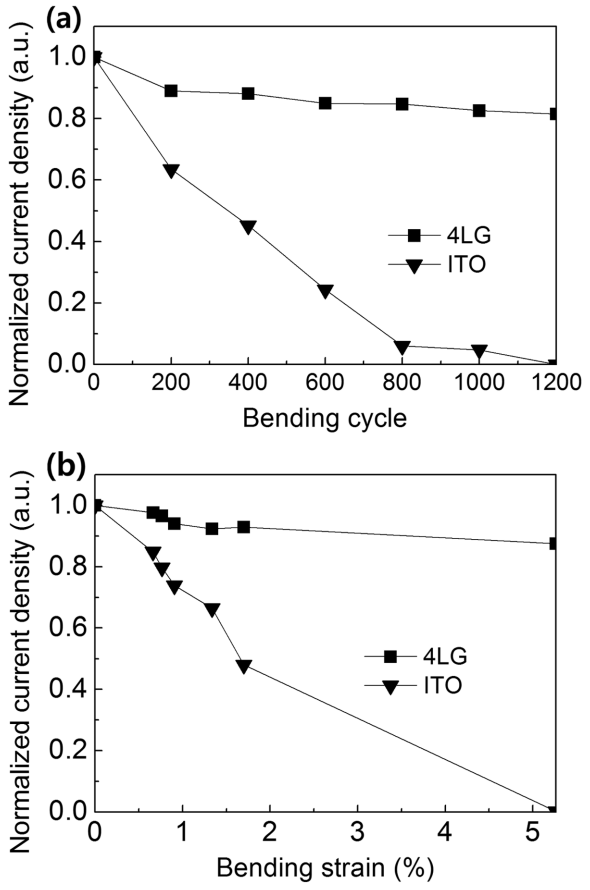

Figure 5. Normalized current density of flexible Gr- and ITO-PeLEDs on PET substrate according to a) bending cycle (bending strain: 1.34%, bending radius: ≈7.5 mm) and b) bending strain.

To conclude, we have developed the first ITO-free organic/inorganic hybrid PeLEDs using a graphene anode. They achieved high CE_{max} = 18.0 cd A^{-1} and EQE_{max} = 3.8%, which are both higher than those of ITO-PeLEDs. We confirmed that the use of graphene anode can avoid formation of exciton quenching sites caused by the diffused In and Sn atoms from ITO anode to the overlying layers. Reduction of exciton quenching by using the chemically inert graphene anode for the $MAPbBr_3$ emitter which has long L_D resulted in increase of device efficiency. In this regard, graphene is a promising anode material to solve the intrinsic problems of organic–inorganic hybrid perovskite emitters based on ITO anodes. We have also fabricated highly flexible Gr-PeLEDs on PET substrate; the graphene anode withstood repeated bending (>1000 bending cycles) and high bending strain (5.3%). Therefore, graphene enables high-efficiency flexible PeLEDs that have high color purity and low fabrication cost, which will provide practical application of next-generation flexible displays and solid-state lighting. We believe that realization of high efficiency PeLEDs using this chemically inert graphene electrode without any metal impurities instead of ITO can open an important research direction to boost the luminous efficiency of PeLEDs. Not only replacing the brittle ITO but also avoiding any exciton quenching centers caused by the ITO electrode is very crucial for achieving high device efficiency in flexible PeLEDs so that the development of flexible electrodes which do not quench excitons in PeLEDs can be obtained.

Experimental Section

Preparation of $MAPbBr_3$ Solution: A mixture of MABr (Dyesol) and $PbBr_2$ (Sigma-Aldrich) in 1.06:1 mol:mol was dissolved (40 wt%) in dimethyl sulfoxide with vigorous stirring. The materials were used as purchased without further purification.

Fabrication of PeLEDs: Patterned 4LG graphene anodes on glass substrate (2.5 cm × 2.5 cm) (or on 200 µm thick PET for flexible Gr-PeLEDs) were doped with HNO_3 vapor for 150 s, then vacuum dried for 20 min. Patterned 4LG and ITO (185 nm) anodes on glass substrates were UV-ozone treated for 10 min. Then a Buf-HIL solution composed of PEDOT:PSS (Clevios P VP AI4083) and tetrafluoroethylene-perfluoro-3,6-dioxa-4-methyl-7-octene-sulfonic acid copolymer (PFI) (Sigma-Aldrich) (1:1 wt:wt), was spin-coated on graphene and ITO anodes at 1500 rpm for 90 s to make a 100 nm thick Buf-HIL layer, and samples were annealed on a hot plate for 30 min at 150 °C in air. Samples were loaded in an N_2 glove box and an $MAPbBr_3$ solution was spin-coated as an emitting layer on Buf-HIL at 3000 rpm for 60 s. During spin-coating, a nanocrystal pinning process using TPBi solution in chloroform was applied.[1] After spin-coating, samples were annealed on a hot plate at 90 °C for 10 min, then loaded in a high-vacuum (5×10^{-7} Torr) chamber for materials deposition. A 50 nm thick TPBi layer was vacuum deposited as an electron injection layer, and LiF (1 nm)/Al (100 nm) were vacuum deposited as cathode layers.

Film Characterization (Raman/SEM/PL/TR-PL/XRD): The Raman data of graphene films were measured using an Alpha 300R Raman spectroscope (WITEC) equipped with a 532 nm diode laser. SEM images were obtained from XL30S FE-SEM (Philips Electron Optics). XRD spectra were measured using a D/MAX-2500/PC X-ray diffractometer (Rigaku). PL spectra were measured using an FP-8300 spectrofluorometer (JASCO) and TR-PL were measured using a time-correlated single photon counting measurement system equipped with a picosecond pulse laser head (LDH-P-C-405B, PicoQuant) with 405 nm excitation wavelength, monochromator (SP-2155, Acton), and ultrafast detection (MCP-PMT (R3809U-50, Hamamatsu)). The PL emission was measured at 545 nm wavelength.

PeLEDs Characterization: The *I–V–L* characteristics were measured using a Keithley 236 source measurement unit and Minolta CS2000 spectroradiometer. Full angular emission characteristics were measured with a motorized goniometer setup equipped with a calibrated photodiode (Thorlab Inc.) and a fiber-optic spectrometer (EPP2000, StellarNet Inc.). The *I–V* characteristics of bending test were measured using a parameter analyzer (Keysight B1500A).

Supporting Information

Supporting Information is available from the Wiley Online Library or from the author.

Acknowledgements

H.-K.S. and H.K. contributed equally to this work. This work was supported by the National Research Foundation of Korea (NRF) grant funded by the Korea government (Ministry of Science, ICT & Future Planning) (Grant No. NRF-2016R1A3B1908431).

Received: October 17, 2016
Revised: December 6, 2016
Published online: January 24, 2017

[1] H. Cho, S.-H. Jeong, M.-H. Park, Y.-H. Kim, C. Wolf, C.-L. Lee, J. H. Heo, A. Sadhanala, N. Myoung, S. Yoo, S. H. Im, R. H. Friend, T.-W. Lee, *Science* **2015**, *350*, 1222.
[2] Y.-H. Kim, H. Cho, J. H. Heo, T.-S. Kim, N. Myoung, C.-L. Lee, S. H. Im, T.-W. Lee, *Adv. Mater.* **2015**, *27*, 1248.
[3] Z.-K. Tan, R. S. Moghaddam, M. L. Lai, P. Docampo, R. Higler, F. Deschler, M. Price, A. Sadhanala, L. M. Pazos, D. Credgington, F. Hanusch, T. Bein, H. J. Snaith, R. H. Friend, *Nat. Nanotechnol.* **2014**, *9*, 687.
[4] a) Y.-H. Kim, H. Cho, T.-W. Lee. *PNAS* **2016**, *113*, 11694; b) G. E. Eperon, S. D. Stranks, C. Menelaou, M. B. Johnston, L. M. Herz, H. J. Snaith, *Energy Environ. Sci.* **2014**, *7*, 982; c) H. Choi, J. Jeong, H. B. Kim, S. Kim, B. Walker, G. H. Kim, J. Y. Kim, *Nano Energy* **2014**, *7*, 80.
[5] S. D. Stranks, G. E. Eperon, G. Grancini, C. Menelaou, M. J. P. Alcocer, T. Leijtens, L. M. Herz, A. Petrozza, H. J. Snaith, *Science* **2013**, *342*, 341.
[6] Y.-C. Hsiao, T. Wu, M. Li, Q. Liu, W. Qin, B. Hu, *J. Mater. Chem. A* **2015**, *3*, 15372.
[7] G. Li, Z.-K. Tan, D. Di, M. L. Lai, L. Jiang, J. H.-W. Lim, R. H. Friend, N. C. Greenham, *Nano Lett.* **2015**, *15*, 2640.
[8] N. K. Kumawat, A. Dey, K. L. Narasimhan, D. Kabra, *ACS Photonics* **2015**, *2*, 349.
[9] J. Wang, N. Wang, Y. Jin, J. Si, Z.-K. Tan, H. Du, L. Cheng, X. Dai, S. Bai, H. He, Z. Ye, M. L. Lai, R. H. Friend, W. Huang, *Adv. Mater.* **2015**, *27*, 2311.
[10] J. C. Yu, D. B. Kim, G. Baek, B. R. Lee, E. D. Jung, S. Lee, J. H. Chu, D.-K. Lee, K. J. Choi, S. Cho, M. H. Song, *Adv. Mater.* **2015**, *27*, 3492.
[11] J. Byun, H. Cho, C. Wolf, M. Jang, A. Sadhanala, R. H. Friend, H. Yang, T.-W. Lee, *Adv. Mater.* **2016**, *28*, 7515.
[12] A. Kumar, C. Zhou, *ACS Nano* **2010**, *4*, 11.
[13] T.-H. Han, M.-R. Choi, S.-H. Woo, S.-Y. Min, C.-L. Lee, T.-W. Lee, *Adv. Mater.* **2012**, *24*, 1487.
[14] T.-H. Han, Y. Lee, M.-R. Choi, S.-H. Woo, S.-H. Bae, B. H. Hong, J.-H. Ahn, T.-W. Lee, *Nat. Photonics* **2012**, *6*, 105.
[15] M. P. de Jong, L. J. van Ijzendoom, M. J. A. Voigt, *Appl. Phys. Lett.* **2000**, *77*, 2255.
[16] A. Sharma, G. Andersson, D. A. Lewis, *Phys. Chem. Chem. Phys.* **2011**, *13*, 4381.
[17] S. G. R. Bade, J. Li, X. Shan, Y. Ling, Y. Tian, T. Dilbeck, T. Besara, T. Geske, H. Gao, B. Ma, K. Hanson, T. Siegrist, C. Xu, Z. Yu, *ACS Nano* **2015**, *10*, 1795.
[18] M. Kaltenbrunner, G. Adam, E. D. Glowacki, M. Drack, R. Schwodiauer, L. Leonat, D. H. Apaydin, H. Groiss, M. C. Scharber, M. S. White, N. S. Sariciftci, S. Bauer, *Nat. Mater.* **2015**, *14*, 1032.
[19] C. Roldan-Carmona, O. Malinkiewicz, A. Soriano, G. Minguez Espallargas, A. Garcia, P. Reinecke, T. Kroyer, M. I. Dar, M. K. Nazeeruddin, H. J. Bolink, *Energy Environ. Sci.* **2014**, *7*, 994.
[20] J. Han, S. Yuan, L. Liu, X. Qiu, H. Gong, X. Yang, C. Li, Y. Hao, B. Cao, *J. Mater. Chem. A* **2015**, *3*, 5375.
[21] Z. Li, S. A. Kulkarni, P. P. Boix, E. Shi, A. Cao, K. Fu, S. K. Batabyal, J. Zhang, Q. Xiong, L. H. Wong, N. Mathews, S. G. Mhaisalkar, *ACS Nano* **2014**, *8*, 6797.
[22] J. Troughton, D. Bryant, K. Wojciechowski, M. J. Carnie, H. Snaith, D. A. Worsleya, T. M. Watson, *J. Mater. Chem. A* **2015**, *3*, 9141.
[23] H. Sung, N. Ahn, M. S. Jang, J.-K. Lee, H. Yoon, N.-G. Park, M. Choi, *Adv. Energy Mater.* **2016**, *6*, 1.
[24] A. K. Geim, K. S. Novoselov, *Nat. Mater.* **2007**, *6*, 183.
[25] H.-K. Seo, T.-S. Kim, C. Park, W. Xu, K. Baek, S.-H. Bae, J.-H. Ahn, K. Kim, H. C. Chio, T.-W. Lee, *Sci. Rep.* **2015**, *5*, 16710.
[26] H.-K. Seo, M.-H. Park, Y.-H. Kim, S.-J. Kwon, S.-H. Jeong, T.-W. Lee, *ACS Appl. Mater. Interfaces* **2016**, *8*, 14725.
[27] H. Kim, J. Byun, S.-H. Bae, T. Ahmed, J.-X. Zhu, S.-J. Kwon, Y. Lee, S.-Y. Min, C. Wolf, H.-K. Seo, J.-H. Ahn, T.-W. Lee, *Adv. Energy Mater.* **2016**, *6*, 1600172.
[28] H. Kim, S.-H. Bae, T.-H. Han, K.-G. Lim, J.-H. Ahn, T.-W. Lee, *Nanotechnol.* **2014**, *25*, 014012.
[29] H. Park, I.-J. Park, D. Y. Jung, K. J. Lee, S. Y. Yang, S.-Y. Choi, *2D Mater.* **2016**, *3*, 021003.
[30] J. O. Hwang, D. H. Lee, J. Y. Kim, T. H. Han, B. H. Kim, M. Park, K. No, S. O. Kim, *J. Mater. Chem.* **2011**, *21*, 3432.
[31] P.-H. Ho, C.-H. Chen, F.-Y. Shih, Y.-R. Chang, S.-S. Li, W.-H. Wang, M.-C. Shih, W.-T. Chen, Y.-P. Chiu, M.-K. Li, Y.-S. Shih, C.-W. Chen, *Adv. Mater.* **2015**, *27*, 7809.
[32] P. You, Z. Liu, Q. Tai, S. Liu, F. Yan, *Adv. Mater.* **2015**, *27*, 3632.
[33] F. Lang, M. A. Gluba, S. Albrecht, J. Rappich, L. Korte, B. Rech, N. H. Nickel, *J. Phys. Chem. Lett.* **2015**, *6*, 2745.
[34] M. Acik, S. B. Darling, *J. Mater. Chem. A* **2016**, *4*, 6185.
[35] M. Batmunkh, C. J. Shearer, M. J. Biggs, J. G. Shapter, *J. Mater. Chem. A* **2016**, *4*, 2605.
[36] X. S. Li, Y. W. Zhu, W. W. Cai, M. Borysiak, B. Y. Han, D. Chen, R. D. Piner, L. Colombo, R. S. Ruoff, *Nano Lett.* **2009**, *9*, 4359.
[37] Y.-K. Chih, J.-C. Wang, R.-T. Yang, C.-C. Liu, Y.-C. Chang, Y.-S. Fu, W.-C. Lai, P. Chen, T.-C. Wen, Y.-C. Huang, C.-S. Tsao, T.-F. Guo, *Adv. Mater.* **2016**, *28*, 8687.
[38] T.-H. Han, W. Song, T.-W. Lee, *ACS Appl. Mater. Interfaces* **2015**, *7*, 3117.
[39] T.-H. Han, Y.-H. Kim, M. H. Kim, W. Song, T.-W. Lee, *ACS Appl. Mater. Interfaces* **2016**, *8*, 6152.
[40] T.-W. Lee, Y. Chung, O. Kwon, J.-J. Park, *Adv. Funct. Mater.* **2007**, *17*, 390.
[41] R. Meerheim, R. Nitsche, K. Leo, *Appl. Phys. Lett.* **2008**, *93*, 043310.
[42] Z. Suo, E. Y. Ma, H. Gleskova, S. Wagner, *Appl. Phys. Lett.* **1999**, *74*, 1177.
[43] M.-S. Lee, K. Lee, S.-Y. Kim, H. Lee, J. Park, K.-H. Choi, H.-K. Kim, D.-G. Kim, D.-Y. Lee, S. Nam, J.-U. Park, *Nano Lett.* **2013**, *13*, 2814.
[44] S. I. Park, J. H. Ahn, X. Feng, S. Wang, Y. Huang, J. A. Rogers, *Adv. Funct. Mater.* **2008**, *18*, 2673.